Vibrational characterization of a high-density Ru(001)-(2×2)-(NO+3O) phase

K. L. Kostov,* D. Menzel, and W. Widdra†
Physik-Department E20, Technische Universität München, D-85747 Garching, Germany
(Received 11 January 2000)

High-density (NO+O) coadsorbate layers on Ru(001) have been studied for oxygen precoverages, Θ_O, between 0.5 and 1 ML by means of high-resolution electron energy loss spectroscopy and temperature programmed desorption. In this oxygen coverage range NO adsorption is possible on any remaining hcp threefold-coordinated site, to a saturation coverage of $\Theta_O+\Theta_{NO}=1$. On the well-ordered (2×2)-3O oxygen layer ($\Theta_O=0.75$ ML) NO molecules adsorb at 90 K with a high sticking coefficient close to unity up to the saturation coverage of 0.25 ML. The NO sublayer is ordered as the NO's occupy the threefold sites of the (2×2) hole structure within the (2×2)-3O mesh conserving the same symmetry. For this well-ordered Ru(001)-(2×2)-(NO+3O) layer the external and internal NO stretching modes show downward dispersions of 16 and 23 cm^{-1}, respectively, from the $\bar{\Gamma}$ point to the $\bar{K}'$ point at the boundary of the surface Brillouin zone. The dispersion of the internal mode can be completely described by dynamical dipole-dipole coupling. This coupling is also dominant for the external mode dispersion for which additional substrate-mediated contributions exist. Based on this understanding of the dynamical coupling the chemical shift of the NO internal and external stretch is determined for various (NO+O) structures. It can be related to the occupation of nearest- and next-nearest-neighbor sites. The internal mode shows chemical shifts between 12 and 30 cm^{-1} per neighboring NO or O but is insensitive to the structure beyond the nearest neighbors. For the external mode significant chemical shifts due to the occupation of the next-nearest-neighbor sites have been determined.

I. INTRODUCTION

Because of its remarkable catalytic features ruthenium has been the object of intense experimental as well as theoretical studies using the modern methods of surface analysis. To understand its catalytic properties, which exhibit often contrasting activities in UHV and under high-pressure conditions,[1,2] careful model investigations of the adsorption of simple molecules like O_2, NO, and CO, as well as their coadsorption are necessary.[3–8] Many surface-sensitive methods, especially electron spectroscopies such as high-resolution electron energy loss spectroscopy (HREELS), x-ray photoelectron spectroscopy (XPS), or low-energy electron diffraction (LEED), require UHV conditions. Often catalytic experiments are therefore separated from real, high-pressure conditions by many orders of pressure, the so-called ''pressure gap.'' This limitation can be partly removed using high-exposure experiments that have led to the discovery of new adsorbate structures. For example, on Ru(001) for oxygen exposures up to 6 L (1 langmuir=1 L=10^{-6} Torr s) well-ordered (2×2)-O and (2×1)-O layers develop consecutively with corresponding coverages of 0.25 and 0.5 ML, respectively.[9–11] Using high oxygen exposures[12] or atomic oxygen from dissociation of NO_2,[13] higher oxygen coverages up to 1 ML can be prepared with formation of an ordered (1×1) layer for 1 ML.[12,14,15] Recently we have discovered and characterized by HREELS and scanning tunneling microscopy (STM) an additional well-ordered intermediate oxygen layer with a coverage of 0.75 ML.[16] This layer exhibits a (2×2) LEED pattern similar to the ordered oxygen structures at 0.25 ML. However the unit cell contains three oxygen adatoms. Since the (1×1)-O layer passivates efficiently the Ru(001) surface for CO or NO postadsorption, only the high-density (2×2)-3O layer gives the possibility to study coadsorption in the oxygen high-coverage regime. The purpose of the present work is to characterize NO postadsorption onto this new oxygen layer. It is a further extension of the geometrical and vibrational studies of NO adsorption onto (2×2)-O and (2×1)-O layers that have been carried out in our institute.[6,17]

On the clean Ru(001) surface NO forms a variety of adsorption complexes depending on the NO coverage.[5,18,19] Finally, at saturation coverage ($\Theta_{NO}=0.75$ ML) a layer with (2×2) symmetry is found with three NO molecules in three different sites of the unit cell: threefold hcp, threefold fcc, and on top[20,21]. The presence of ordered (2×2)-O or (2×1)-O layers leads to on-top and threefold-adsorbed NO with formation of four different coadsorbate structures: (2×1)-(NO+O), (2×2)-(NO+2O), (2×2)-(2NO+O), and (2×2)-(NO+O).[4] For (2×2)-O on-top and threefold (fcc) adsorbed NO molecules are found by quantitative LEED measurements[4] in agreement with vibrational data.[17] Here the oxygen atoms occupy—with and without coadsorbed NO—threefold hollow sites. Upon low-temperature (150 K) NO adsorption on an (2×1)-O layer, NO molecules occupy only the threefold hcp sites between the (2×1)-O rows.[6] Annealing this layer to 430 K leads to partial NO desorption and rearrangement of the oxygen adatoms, resulting in a well-ordered honeycomb structure. Here the NO molecules are localized in on-top sites, each surrounded by six oxygen adatoms.[4] In this study we show that for NO adsorption on the (2×2)-3O layer no rearrangement of the oxygen layer is observed during thermal desorption, in contrast to NO adsorption on the (2×1)-O layer. The NO molecules are adsorbed on strongly localized sites with a sticking probability close to unity. The structural and vibrational

features of the adsorbed NO in this dense oxygen layer are the subject of the present work. Using different NO+O high coverage-structures the influence of nearest- and next-nearest neighbor atoms on the internal and external NO stretching frequencies (their chemical shifts) will be discussed.

II. EXPERIMENT

The experiments were carried out in a two-level UHV system at a base pressure of 4×10^{-11} mbar. On the lower chamber it houses a HREEL spectrometer (Delta 05, VSI) with a best resolution of 5.7 cm^{-1} at an intensity of the specularly reflected beam of 1×10^{5} s^{-1} for the Ru(001) surface. The vibrational spectra presented here have been performed with a resolution of about 8 cm^{-1}, corresponding to count rates up to 10^{6} s^{-1}. More details are given elsewhere.[15] The upper (preparation) chamber is equipped with LEED, XPS, Kelvin probe, and temperature programmed desorption (TPD) facilities. The thermal desorption equipment consists of a quadrupole mass spectrometer (Balzers QMS 112) with a Feulner cup that allows quantitative reproducibility of the TPD spectra to a few percent.[22] During the NO adsorption onto the Ru(001)-(2×2)-3O layer and also NO desorption, the work-function changes were monitored using a Kelvin probe with an experimental accuracy of about 1 meV.[23]

The Ru crystal was cleaned by standard procedures including initial Ar-sputtering followed by heating in UHV and in oxygen pressures of about 10^{-7} mbar. Between experiments only several heating cycles up to 1400 K in oxygen and annealing to 1570 K in UHV are necessary to produce a clean surface as was monitored mainly by HREELS. The gas dosing for the HREELS and TPD experiments were carried out in front of a microcapillary array in order to ensure homogenous coverages.

III. RESULTS

A. NO adsorption onto oxygen-covered Ru(001), $\Theta_O \geq 0.5$ ML

Figure 1 shows HREEL spectra for the oxygen-covered Ru(001) surface in the range from $\Theta_O=0.5$ to 1.0 ML, Figs. 1(a) to 1(g), respectively. The spectra have been recorded in energy loss steps of 1.56 cm^{-1} and a total measurement time of 1 s per channel for spectra (a) to (f). Spectrum (g) has been measured with 0.5 s per channel. The vibrational spectrum for the (2×1)-O layer at $\Theta_O=0.5$ ML, Fig. 1(a), is in good agreement with previous work with lower resolution.[24,25] The asymmetric line shape of the O-Ru stretching vibration results from an oxygen coverage slightly above 0.5 ML. The additional oxygen atoms lead to a shoulder at about 600 cm^{-1}. With increasing oxygen coverages, Figs. 1(b) and 1(c), the appearance of two new losses at 541–547 and 632–637 cm^{-1} indicates the growth of a new phase. This new phase is completed as soon as the loss feature due to the (2×1)-O domains at 580 to 588 cm^{-1} disappears. It corresponds to the well-ordered (2×2)-3O phase at a coverage of 0.75 ML as discussed elsewhere.[16] For the optimal (2×2)-3O structure both peaks at 641 and 550 cm^{-1}, Fig. 1(e), exhibit maximal intensities and smallest widths. They have been attributed to the O-Ru stretching vibration and the dipole-active frustrated translation parallel

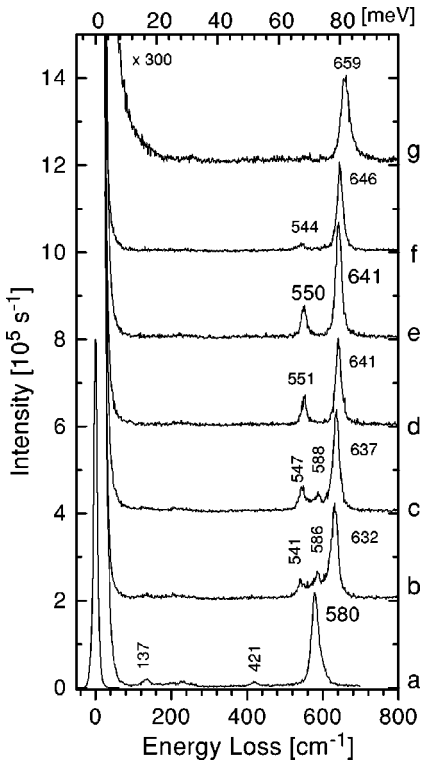

FIG. 1. HREEL spectra for different oxygen coverages on Ru(001): (a) ≈0.5 ML; (b) 0.57 ML; (c) 0.65 ML; (d) 0.71 ML; (e) 0.75 ML; (f) 0.85 ML; (g) 0.97 ML.

to the surface (breathing motion) of the three oxygen adatoms within the unit cell, respectively.[16] A further increase of the oxygen coverage as shown in Figs. 1(f) and 1(g) leads to a frequency shift of the ν(O-Ru) stretch up to 660 cm^{-1} as for the ideal (1×1)-O layer[15] which is accompanied by a decrease of the 550 cm^{-1} loss intensity due to remnant (2×2)-3O domains. Note that the resolution in Fig. 1(g) is slightly degraded to about 12 cm^{-1} and that the tail of the elastic peak extends to higher energies. Therefore one has to be careful comparing loss intensities between spectrum (g) and the others.

HREEL spectra after NO saturation at 90 K for the seven different Ru(001)-O layers of Fig. 1 are shown in Fig. 2. Subsequent NO thermal desorption data for these coadsorption layers are displayed in Fig. 3. The results for NO adsorption onto the (2×1)-O layer, $\Theta_O=0.5$ ML, Figs. 2(a) and 3(a),[26] are in good agreement with previous infrared and TPD data of Jakob *et al.*[6] Here, NO is adsorbed in the threefold hcp sites between the (2×1)-O rows. Due to the (2×1) domain boundaries a small amount of NO ($\Theta_{NO}<4\%$) adsorbs in on-top positions.[6] We observe both species with ν(N-O) stretching modes at 1614 and 1839 cm^{-1}, respectively. Compared to Ref. 6 more details are visible in the low-frequency region: The ν(Ru-NO) stretching mode is observed at 435 cm^{-1}. Additionally, a loss feature is detected around 490 cm^{-1}, which is attributed to the dipole-active O-Ru out-of-row bending mode based on isotope experiments as discussed in detail elsewhere.[27] The O-Ru stretching mode is strongly attenuated by the NO and not visible here. Spectra with better counting statistics clearly show this mode at 628 cm^{-1} for the (2×1)-(NO+O) layer.[27] The structural model based on the vibrational data

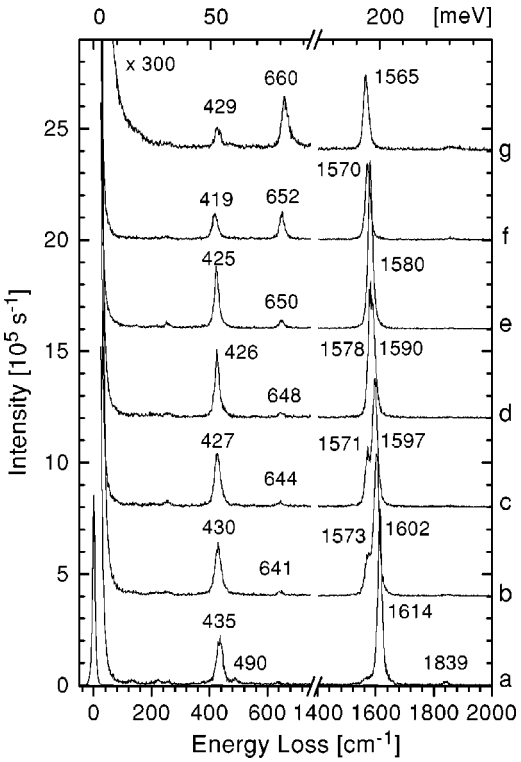

FIG. 2. HREEL spectra for the layers shown in Fig. 1 after saturation with NO at 90 K.

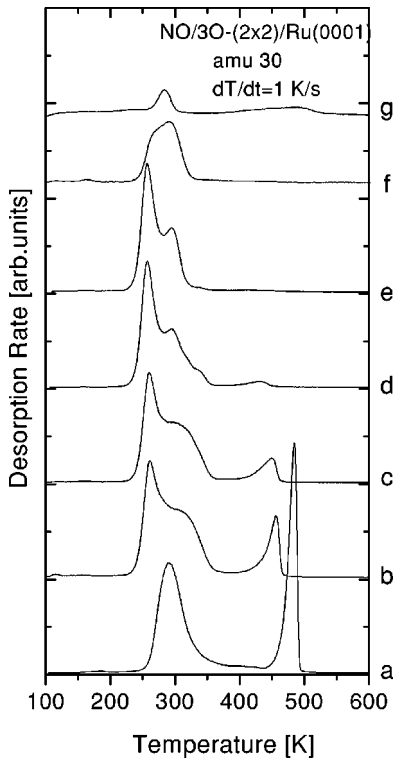

FIG. 3. Thermal desorption spectra of molecular NO desorbing from the layers presented in Fig. 2. The NO coverages were determined (see also text) to be (a) 0.5 ML; (b) 0.43 ML; (c) 0.35; (d) 0.29 ML; (e) 0.25 ML; (f) 0.15 ML; (g) 0.03 ML.

that has been confirmed by a quantitative LEED study gives a NO coverage of 0.5 ML for the saturated and ordered (2×1)-(NO+O) layer at low temperatures.[4,6] We will use this value to estimate the absolute NO coverages for all other layers. Assuming complete molecular NO desorption the corresponding NO coverages in Figs. 2 and 3 from (a) to (g) are 0.50, 0.43, 0.35, 0.29, 0.25, 0.15, and 0.03 ML, respectively. Based on this NO coverage determination of $\Theta_{NO}=0.25$ in Fig. 3(e) it follows immediately that NO can adsorb in all vacant hcp sites of the (2×2)-3O structure, forming a well-ordered (2×2)-(NO+3O) structure. As we will show below the assumption of complete molecular desorption is valid for the (2×2)-(NO+3O) structure. In the case of the (2×1)-(NO+O) layer a small amount of NO dissociation has been reported.[6] It depends on the quality of the (2×1)-O layer and is here estimated to be about 4%. From the fact that all hcp sites of the (2×1)-O and (2×2)-3O layers can be saturated by NO and also vacant hcp sites for oxygen coverages above $\Theta_O>0.75$ ML are accessible to NO [see Figs. 2(f), 2(g), 3(f), and 3(g)], it is straightforward to assume that in all cases (for oxygen coverages $\Theta_O\geqslant0.5$) the total coverage upon NO saturation is unity, $\Theta_O+\Theta_{NO}=1$. The corresponding different partial coverages are indicated in the captions of the figures. The particular form of the thermal desorption spectrum for the (2×1)-(NO+O) layer, Fig. 3(a), has been discussed previously.[7] Its high-temperature (>350 K) region corresponds to a rearrangement of the oxygen atoms and the remaining NO molecules to a honeycomb (2×2)-(NO+2O) structure with the NO positioned in on-top sites.[4,6]

Increasing the oxygen precoverage above 0.5 ML a second internal N-O stretching mode appears at a lower frequency <1580 cm^{-1} as can be seen in Figs. 2(b)–2(d). It can be attributed to NO molecules localized in (2×2)-3O domains, i.e., NO molecules that are surrounded by six oxygen atoms. As is seen in Figs. 3(a)–3(d) the thermal desorption peak of the linearly bonded NO above 400 K decreases strongly, which can be explained as due to the increase of the (2×2)-3O domain area. The high-temperature peak is not observed for an ideal (2×2)-3O layer [Fig. 3(e)]. For the latter layer only one narrow ν(N-O) peak at 1580 cm^{-1} exists; see Fig. 2(e). The two-peak structure of its TPD spectrum in Fig. 3(e) is interpreted purely by NO-NO lateral interactions, which contain a nearest-neighbor repulsion as well as an attractive trio interaction as will be discussed in more detail together with lattice gas simulations elsewhere.[28]

A further increase of the oxygen coverage above 0.75 ML decreases the amount of adsorbed NO, [Figs. 3(f) and 3(g)], and shifts the ν(N-O) stretch down to 1565 cm^{-1} for a layer with $\Theta_O=0.97$ and $\Theta_{NO}=0.03$. It is most probably characteristic for NO molecules localized in isolated vacant threefold sites in the (1×1)-O mesh. As seen from Fig. 2(a), a strong screening of the O-Ru stretch at 580 cm^{-1} is observed after NO postadsorption for the (2×1)-O layer. The intensity of the O-Ru stretch peak increases with decreasing NO coverage; simultaneously a blue shift of the ν(O-Ru) loss is observed (Fig. 2). On an almost saturated (1×1)-O layer [Fig. 2(g)], ν(O-Ru)$=660$ cm^{-1} is measured; the same value has been recently reported for a fully saturated pure Ru(001)-(1×1)-O layer.[15]

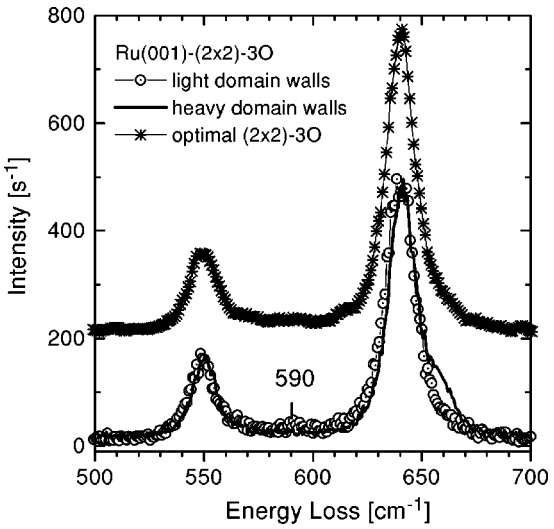

FIG. 4. Detailed HREEL spectra for the (2×2)-3O structure on Ru(001): The spectrum for an ideal (2×2)-3O layer is marked by stars. Spectra corresponding to slightly higher and lower oxygen coverages than the ideal (2×2)-3O structure (0.75 ML) are marked as solid line and by circles, respectively.

B. NO adsorption on the ideal Ru(001)-(2×2)-3O layer

1. Preparation of an optimal saturated (2×2)-3O coverage

We control the formation of a well-ordered defect-free (2×2)-3O layer by means of HREELS and TPD. As has been discussed for Figs. 1(b) to 1(d), the remaining (2×1)-O-like domains are characterized by a third oxygen loss at 586–590 cm^{-1}. This peak disappears with the completion of the ordered (2×2)-3O phase. Our significantly improved resolution (about 1 meV) allows us to monitor the frequency region between 550 and 640 cm^{-1} in detail, as is demonstrated in Fig. 4. The existence of missing oxygen atoms (below 0.02 ML) within the (2×2)-3O layer can be monitored by a low-intensity peak at about 590 cm^{-1}. This implies a local environment containing oxygen atoms with only three nearest-neighbor oxygen atoms. On the other hand, at an oxygen coverage slightly above 0.75 ML a shoulder (at about 660 cm^{-1}) on the higher-energy side of the O-Ru stretching loss at 640 cm^{-1} is detectable, which might be interpreted as additional oxygen atoms (with five or six oxygen nearest-neighbor atoms) within the layer. Since individual (2×2)-3O domains can have an offset of half a (2×2) unit cell against each other, the existence of domain boundaries is most likely. These domain boundaries form stripes of either higher or lower local coverage, i.e., containing oxygen atoms with 3 or 5 nearest-neighbor oxygen atoms, respectively. Therefore the additional losses at 590 and 660 cm^{-1} shown in Fig. 4 are likely to correspond to light and heavy domain walls, respectively. As we discussed here HREELS is very sensitive to the formation of the ideal (2×2)-3O layer, which can be optimized by additional oxygen adsorption or desorption. An alternative method based on thermal desorption spectra of coadsorbed NO will be discussed in the next section.

2. Preparation of the ideal (2×2)-(NO+3O) coadsorption layer

As mentioned in Sec. III A the study of NO coadsorption gives information about the structure of the dense oxygen layers on Ru(001). Figure 5 shows NO TPD spectra from NO saturated NO+O layers for a series of oxygen precoverages between 0.7 and 0.75 ML. The dominant two desorption features that agree well with the spectrum in Fig. 3(e) are characteristic for the ideal (2×2)-(NO+3O) layer. However, for slightly lower oxygen coverages two additional NO desorption features around 330–340 and 420–440 K are clearly visible. With oxygen coverages decreasing below 0.75 ML first the 340 K peak grows. Subsequently the desorption peak at 420–440 K develops, which might be interpreted as NO desorption out of small reconstructed honeycomblike areas where one on-top NO is surrounded by six oxygen atoms. The latter interpretation is supported by the analogy with NO desorption at $\Theta_O=0.5$ ML; see Figs. 3(a) to 3(d). From the TPD spectra in Fig. 5 it follows that this higher-temperature peak decreases and vanishes when the oxygen precoverage approaches $\sim$0.72 ML. Therefore up to this value small (2×1)-O domains exist. Between 0.72 and 0.75 ML mainly a shoulder at about 340 K is visible. In view of the discussion above it is attributed to NO desorption out of light domain walls or NO sites at an oxygen vacancy within the (2×2)-3O. In the absence of (2×1)-O rows the dense NO+O layer cannot reconstruct to the honeycomb structure for geometrical reasons. In conclusion, the shape of the high-temperature edge of the NO thermal desorption spectrum is a reliable indicator for the perfection of the Ru(001)-(2×2)-(NO+3O) layer.

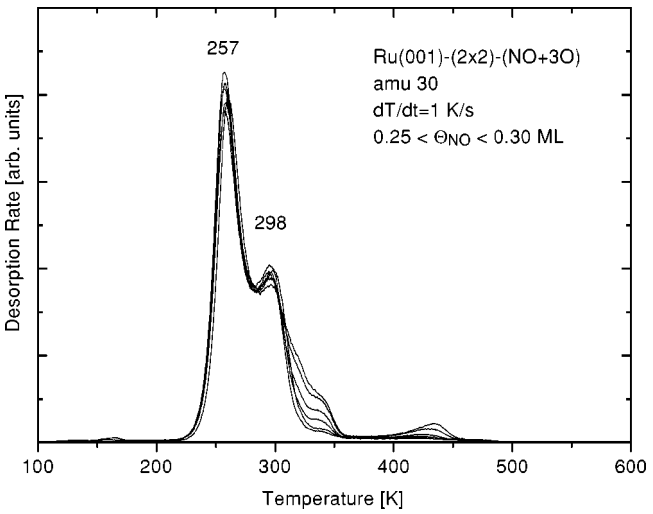

FIG. 5. Thermal desorption spectra of molecular NO from saturated NO+O layers for different oxygen precoverages between 0.70 and 0.75 ML.

C. Vibrational results

NO postadsorption at 100 K onto the oxygen covered Ru(001)-(2×2)-3O layer reveals a high sticking coefficient close to unity up to saturation and causes a work-function increase of $\Delta\Phi=0.190\pm0.005$ eV. As follows from the vibrational data shown below, NO is adsorbed only in one chemisorbed state, and weak dynamical interactions with the other NO neighbors exist. Up to saturation of the NO sublayer the work-function changes linearly with exposure. Therefore the existence of a weakly bound precursor state can be assumed. The $\Delta\Phi$ and TPD data will be discussed elsewhere together with detailed kinetic modeling.[28]

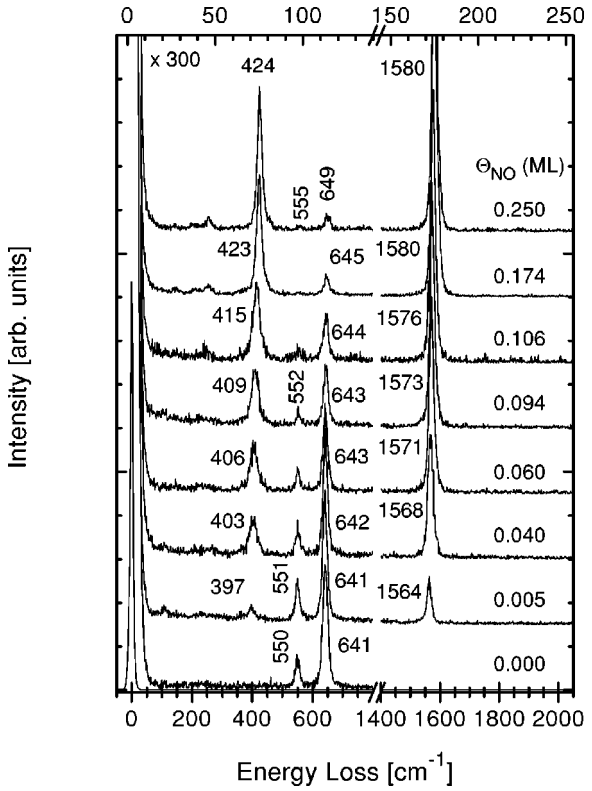

FIG. 6. HREEL spectra of different NO coverages (Θ_{NO}) on an optimal Ru(001)-(2×2)-3O layer.

In Fig. 6 HREEL spectra for different exposures to NO of an optimal Ru(001)-(2×2)-3O layer at 96 K are shown. The indicated NO coverages have been determined from subsequent TPD spectra assuming a saturation value of 0.25 ML (see Sec. III A). With increasing NO coverage two intense losses grow and undergo shifts to higher frequencies. At saturation the peaks that are attributed to the ν(Ru-NO) and the ν(N-O) stretching vibrations of threefold-coordinated NO are located at 424 and 1580 cm^{-1}. With increasing NO coverage the characteristic losses of the (2×2)-3O layer at 550 and 641 cm^{-1} are strongly attenuated and shift up to 555 and 649 cm^{-1} for the saturated (2×2)-(NO+3O) layer.

Figure 7 displays the vibrational spectrum of the (2×2)-(NO+3O) layer with more details. Besides the dominating modes already discussed, two additional modes can be observed in the region above 3000 cm^{-1}: the features at 3094 and 3160 cm^{-1} are interpreted as the overtone and the double loss of the N-O stretch at 1580 cm^{-1}, respectively. In the low-energy region of the substrate phonons we detect three peaks at 146, 207, and 255 cm^{-1} in contrast to the observation for the pure (2×2)-3O layer.[16] They can be attributed to the Rayleigh mode and two longitudinal phonons, respectively, which are back-folded from the $\bar{M}$ point of the (1×1) surface Brillouin zone[29] due to the presence of the (2×2) adsorbate overlayer.[25] This back-folding is strong for the (2×2)-(NO+3O) but hardly visible for the (2×2)-3O layer, indicating that the (2×2) Fourier components that cause the back-folding increase with NO adsorption.

During annealing of the saturated (2×2)-(NO+3O) layer no dissociation of NO is observed. This is obvious

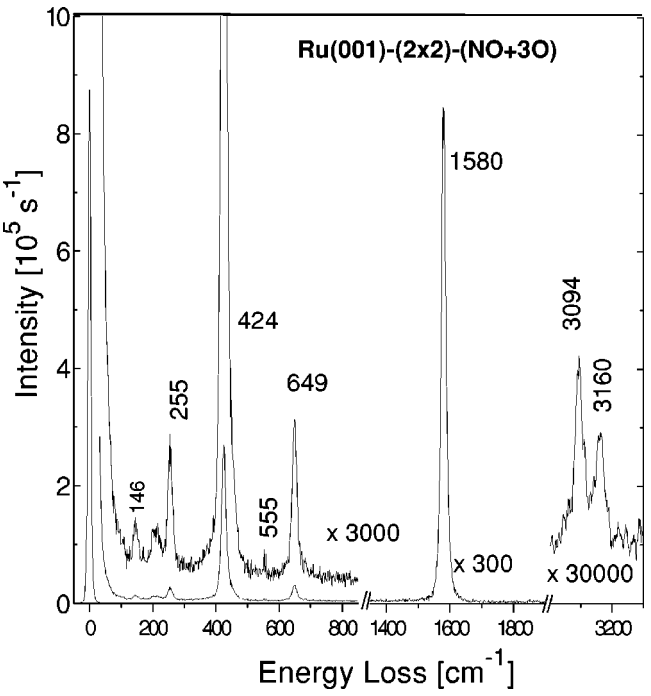

FIG. 7. Vibrational spectrum of the well-ordered Ru(001)-(2×2)-(NO+3O) layer: Θ_{NO}=0.25 ML and Θ_O=0.75 ML.

from the experimental data shown in Fig. 8. After NO saturation at 100 K and subsequent heating to the indicated temperatures no additional losses to those described above are visible. When NO desorption is completed the characteristic vibrational spectrum of the (2×2)-3O layer is observed as

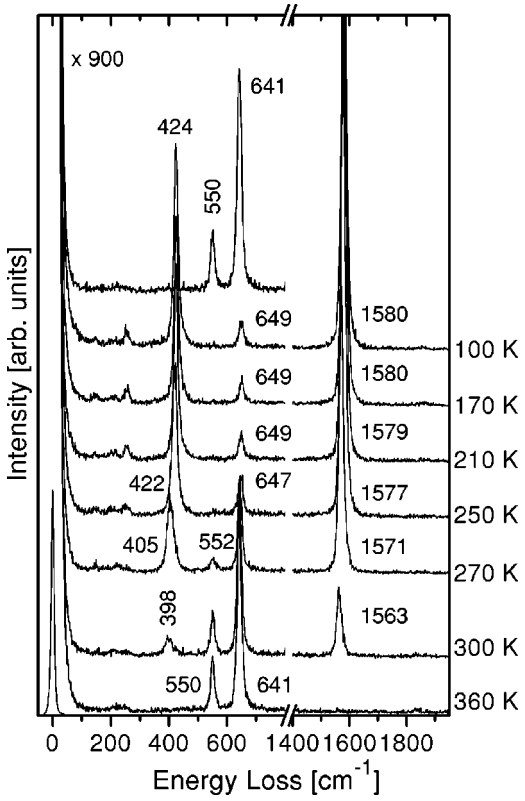

FIG. 8. HREEL spectra for the Ru(001)-(2×2)-(NO+3O) layer after annealing to the indicated temperatures.

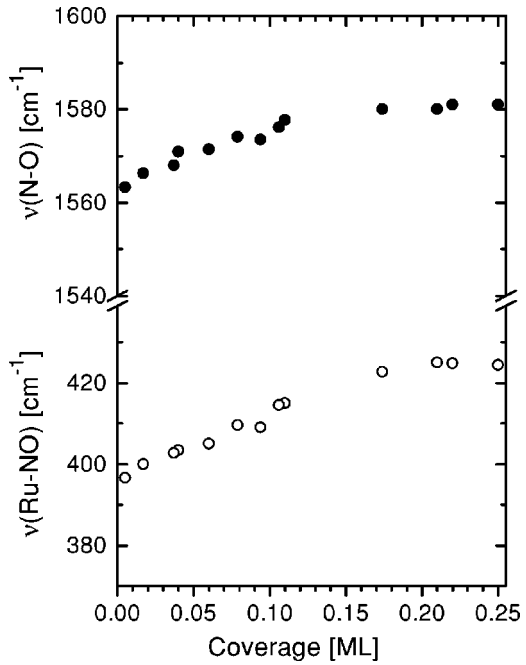

FIG. 9. Vibrational frequencies of the external and internal NO stretching modes versus NO coverage.

before NO adsorption. In view of the discussion in Sec. III A this indicates that no additional oxygen is left upon NO desorption, which excludes any NO dissociation ($<1\%$). Note that at oxygen coverages below 0.75 ML, NO dissociation during annealing is detected based on a shifted O-Ru stretching mode. It is not clear whether the dissociation process can be connected to on-top adsorbed NO species that still exist on the surface at oxygen precoverages below 0.75 ML, or to NO adsorbed in the imperfections (domain walls) of the mixed (2×1)-O and (2×2)-3O phases. We emphasize that the vibrational spectra for all annealing temperatures show the presence of only one threefold adsorbed NO species and a continuous frequency shift of both characteristic Ru-NO and N-O stretching losses versus NO coverage, as compiled in Fig. 9. To address the question if these shifts with NO coverage are due to dynamical coupling within the adlayer or if they represent a chemical shift, the dispersion relation has been mapped out.

So far we have discussed only the vibrational spectra at the $\overline{\Gamma}$ point (no momentum transfer), which are dominated by dipole scattering and where equivalent oscillators of different unit cells vibrate in phase. However, due to dynamical lateral coupling these modes might exhibit frequency shifts with momentum transfer; i.e., show phonon dispersions within the adsorbate Brillouin zone. The dispersion experiments that will be presented have been accomplished in an electron energy range up to 144 eV at a constant scattering angle of 120°. These off-specular measurements were carried out with a scattering geometry corresponding to momentum transfer along the $\overline{\Gamma K' M'}$ direction in reciprocal space, as shown in the inset of Fig. 11. Figure 10 represents some off-specular HREEL spectra for the (2×2)-(NO+3O) layer for an electron energy of 64 eV, apart from the last spectrum at $k_\parallel = 1.149$ Å^{-1}, which has been measured at an electron energy of 100 eV. At higher electron energies, even at the $\overline{\Gamma}$ point, a new loss peak at about 500 cm^{-1} is clearly observed, which shows only weak dispersion. In the absence of NO, for the pure (2×2)-3O layer, such a peak at 500 cm^{-1} had also been found.[30] Therefore we assign this loss to a parallel O-Ru bending mode.

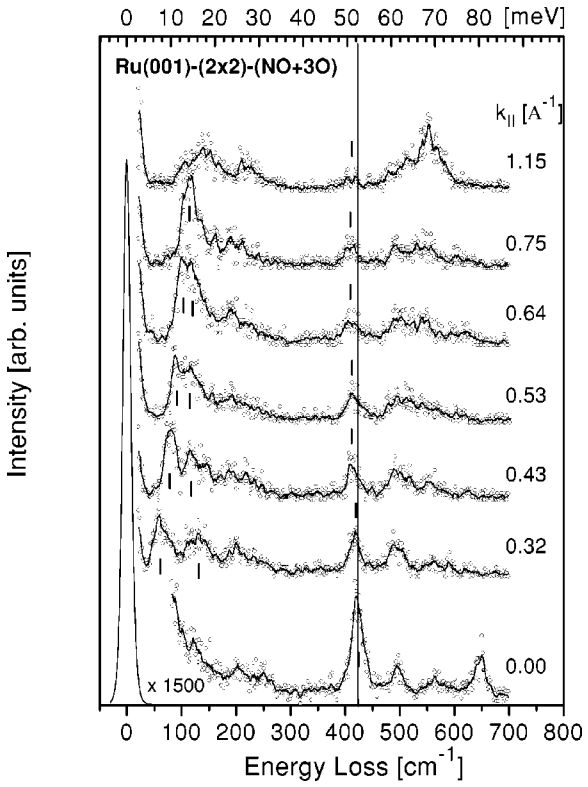

FIG. 10. Off-specular HREEL spectra for the Ru(001)-(2×2)-(NO+3O) layer along $\overline{\Gamma K' M'}$ in the surface Brillouin zone for the indicated parallel momentum transfer.

The external NO stretching mode clearly exhibits a small downward dispersion from 424 to below 410 cm^{-1} with increasing $k_\parallel$. The intense peak in Fig. 10 at lowest frequencies is attributed to the excitation of the Rayleigh phonon.

The results of 35 spectra are compiled in Fig. 11. For the (2×2)-(NO+3O) layer the external and internal NO stretching vibrations exhibit downward dispersions of about 16 and 23 cm^{-1}, respectively, with a minimum frequency for the internal mode around the $\overline{K'}$ point. Both modes show only weak dispersion at higher $k_\parallel$. For the internal mode the dispersion can be well described by long-range dynamical dipole-dipole interactions between the adsorbed NO molecules. The mathematical formalism is adapted from Ref. 31; it has been applied before to explain the steep dispersion of the vertical O-Ru stretching mode of the pure Ru(001)-(1×1)-O layer:[15]

$$\frac{\nu}{\nu_A} = \sqrt{1 + \frac{\alpha_v \sum k_\parallel}{1 + \alpha_e \sum k_\parallel}}, \tag{1}$$

where

$$\sum k_\parallel = \sum_{lattice} \frac{\exp(ik_\parallel r)}{|r|^3}, \tag{2}$$

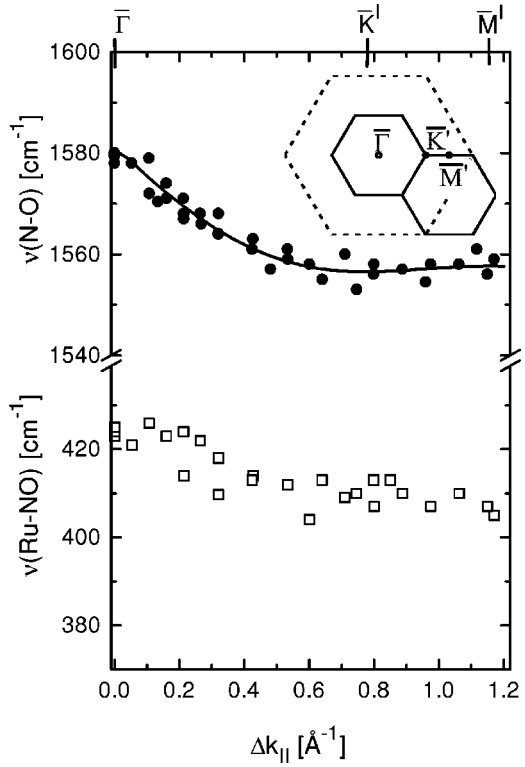

FIG. 11. Dispersion of the external and internal NO stretching modes along $\overline{\Gamma K' M'}$. The inset shows the surface Brillouin zone for the clean surface (dashed line) and the (2×2) overlayer (full line).

ν_A, α_e, and α_v being the frequency of an isolated oscillator (singleton frequency) and the electronic and the vibrational polarizabilities, respectively, and r is the location of the surrounding oscillators in their two-dimensional lattice. The calculation and the different sensitivities of the three parameters have been described in Ref. 15. From the data shown in Fig. 11 values of $\nu_A = 1561.5\ \mathrm{cm}^{-1}$, $\alpha_e = 2\ \text{Å}^3$, and $\alpha_v = 0.42\ \text{Å}^3$ have been extracted. The solid line indicates this fit. The quality of the fit—especially the agreement at the zone boundary—indicates negligible contribution of any short-range interactions, e.g., from surface-mediated coupling. The singleton frequency for the (2×2)-(NO+3O) layer can be compared with the frequency of this mode in the limit of zero NO coverage; see Fig. 9. The agreement of both frequencies within 2 cm^{-1} demonstrates that there is no NO-induced chemical shift for the internal NO stretch. However, for the external mode the zero-coverage limit of 397 cm^{-1} is out of the range of the dispersion of this mode for the (2×2)-(NO+3O) layer. Clearly, for this mode a NO-induced chemical shift (of about 15 cm^{-1}) is established. This emphasizes nicely the fact that external vibrations are more sensitive to changes in the local environment than the internal modes as will be discussed below. Although it seems rather unlikely, in principle a coverage-dependent coupling between the external NO stretch and an oxygen bending mode of proper symmetry might contribute also to this shift.

The last vibrational feature that will be discussed here is the overtone of the NO internal stretch. For the (2×2)-(NO+3O) layer it is clearly visible in Fig. 7 at 3094 cm^{-1} in addition to the double loss at 3160 cm^{-1}. Compared to twice the singleton frequency of the NO internal stretch of 3123 cm^{-1} it is red-shifted by 29 cm^{-1} due to the anharmonicity of the internal bond. Since this value is significantly below the bottom of the narrow two-phonon band at 3113 cm^{-1} the coupling to the two-phonon band is only weak (1.4 cm^{-1} shift). Taking this coupling into account as has been discussed by Jakob and Persson,[32] this leads to an anharmonicity shift of 28 cm^{-1}. This value agrees with the gas-phase value of 28 cm^{-1},[33] and with the value found for NO adsorbed on Ru(001)-(2×1)-O in the limit of zero coverage of 29 cm^{-1}.[17] It therefore indicates an unperturbed anharmonicity of this vibrational potential upon adsorption.

IV. DISCUSSION

A. Dynamical adsorbate-adsorbate interactions in the (2×2)-(NO+3O) layer

Although for the (2×2)-(NO+3O) layer the separation between nearest-neighbor NO molecules is twice the Ru-Ru nearest-neighbor distance with oxygen atoms in between, we have shown that the dynamical lateral interactions lead to measurable dispersions for the NO internal and external stretching modes. The dispersion of 23 cm^{-1} for the internal mode with an initially linear red shift and a minimum at $\overline{K'}$ can be completely described by dynamical dipole-dipole coupling. The extracted polarizabilities can be compared with data for the $c(4\times2)$ NO layer on Ni(111).[34] This layer consists of NO adsorbed in the threefold hollow sites with a coverage of 0.5 ML. For this layer Stirniman *et al.* found for the internal stretch a dispersion with increasing momentum transfer of 120 cm^{-1}, which was fitted by an azimuthally averaged dynamical dipole-dipole coupling with polarizabilities α_v and α_e of about 1.24 and 8.0 Å^3, respectively.[34] The singleton frequency was determined to be 1499 cm^{-1}, not too different from our 1561.5 cm^{-1} for the (2×2)-(NO+3O) layer. However, on the Ni surface their reported NO polarizabilities of about $\alpha_v \approx 1.24\ \text{Å}^3$ and $\alpha_e \approx 8.0\ \text{Å}^3$ strongly deviate from the values of 0.4 and 2 Å^3, respectively, found in our work. Especially the discrepancy in α_v by a factor of 3 is surprising. Due to the presence of three rotational domains on the Ni surface and the limited momentum range of their dispersion data the determination of the electronic polarizability α_e might be less reliable than stated by the authors. Since around the $\overline{\Gamma}$ point α_v and α_e can compensate each other to some extent, which, e.g., can be seen in Eq. (1), the high value for α_e might have implied the high value of α_v. Note that an electronic polarizability of $\alpha_e = 8\ \text{Å}^3$ implies that the depolarization factor $1+\alpha_e\Sigma(k_\parallel)$ reaches about 4 at $\overline{\Gamma}$. This quite unusually high value corresponds to a drop of the dipole scattering intensity to 1/16 compared to the value in the absence of depolarization. Clearly, further studies on the NO polarizabilities for different substrates and in different geometric structures are necessary.

Based on the similarities of the dispersions of the external and the internal stretch vibrations the dynamical dipole-dipole coupling is also likely to be the dominant contribution for the external mode. However, since the data seem to have no minimum at $\overline{K'}$ additional short-ranging substrate-

TABLE I. Singleton frequencies for the external and the internal NO stretching modes of six different layers on Ru(001) that contain exclusively threefold-coordinated NO. The numbers and kinds of next neighbors, (A), and next-nearest neighbors, (B) and (C), for the NO molecule is stated in columns 2 to 4.

Layer	Sites (A)	Sites (B)	Sites (C)	T_z (cm^{-1})	ν(N-O) (cm^{-1})	Refs.
(2×2)-3O+$\Theta_{NO}\rightarrow0$	6O	6O	–	397	1564	This work
(2×2)-(NO+3O)	6O	6O	6NO	415	1562	This work
$\Theta_O\rightarrow1$, $\Theta_{NO}\rightarrow0$	6O	6O	6O	429	1565	This work
(2×1)-(NO+O)	4O+2NO	4O+2NO	6NO	–	1548	27
(2×1)-O+$\Theta_{NO}\rightarrow0$	4O	4O	–	–	1524	17
$\Theta_{NO}\rightarrow0$, $\Theta_O=0$	–	–	–	$\approx$350	$\approx$1400	19

mediated contributions are likely to contribute at the zone boundary. Unfortunately, no dispersion data for the external NO stretching mode on any other single crystal surface are available in the literature for comparison.

B. Chemical shifts and their sensitivities to the local structure

Based on the extracted singleton frequencies which correspond (for dipole-dipole coupling) also to the ''centers of gravity'' of the dispersions, we have shown that the internal NO mode shows no chemical shift with NO coverage: Its frequency of 1562 cm^{-1} is coverage independent in the absence of dynamical coupling. Furthermore, this frequency seems to stay constant even with increasing oxygen coverages (decreasing NO coverages) as discussed in Sec. III C. On the other hand, a different singleton frequency of the internal NO mode for NO adsorbed on an (2×1)-O layer has been determined (1524 cm^{-1}) at low NO coverages,[17] which additionally exhibits a chemical shift with NO coverage.[6] Therefore, the frequency of the NO internal stretch seems to depend on the six nearest-neighbor atoms only. Any change in the population or identities of the next-nearest neighbors does not affect the internal mode within the experimental error. The results for different NO+O coadsorbate layers are summarized in Table I together with a listing of the occupations of the nearest-neighbor and next-nearest-neighbor sites: the sites (A), (B), and (C), respectively. The positions of these different sites are illustrated in Fig. 12. The first three rows in Table I compare three different structures that are identical with respect to the occupation of the neighboring sites (A) and (B) around a central NO molecule. They differ only in the number and kind of adsorbates at site (C): Whereas the internal NO stretch is not sensitive to this difference, the external stretch shifts upwards by 18 and 32 cm^{-1} when these sites are occupied by NO or oxygen, respectively. The assumption of a linear shift with the number of occupied sites (C) results in chemical shifts of 3 and 5 cm^{-1} per NO or O occupied site (C), respectively. The last three rows in Table I summarize data for the singleton frequency of the internal NO stretch for three structures that differ from the first three by the number and kind of nearest-neighbor sites (A). Unfortunately, no corresponding data for the external mode are available in the literature.

For the internal NO stretch we find a significant chemical shift of 165 cm^{-1} between the different structures. Since we have demonstrated that this mode is insensitive to the occupation of site (C) and since the distance to sites (B) and (C) is not very different, it is straightforward to assume that the dominant shift is simply due to sites (A). By comparison of low-coverage NO data that show a stretching mode at about 1400 cm^{-1} with data for low-coverage NO within the (2×1)-O row structure (singleton frequency at 1524 cm^{-1}), we extract a chemical shift of about 4×31 cm^{-1}, i.e., 31 cm^{-1} per neighboring oxygen atom in site (A). By comparing the value for NO at missing oxygen sites in a (1×1)-O layer (1565 cm^{-1}) with the low-coverage NO data within the (2×1)-O row structure, we arrive at a chemical shift of about 1565–1524 $cm^{-1}=2\times20.5$ cm^{-1}, i.e., a reduced value of 21 cm^{-1} per additional neighboring oxygen atom. This indicates a sublinear change of the chemical shift with the number of surrounding oxygen atoms.

From the data of the (2×1)-(NO+O) structure we find an NO-induced shift of about 24 cm^{-1} if compared to the low-coverage NO within the (2×1)-O row structure. This corresponds to a NO induced shift of 12 cm^{-1} per NO molecule at site (A). Note that the oxygen-induced chemical shift is about a factor between 2.6 and 1.8 higher than the NO-induced one, most likely due to its higher electronegativity.

In all cases the filling of empty neighbor sites with increasing coverage leads to a blueshift of the singleton frequencies. These frequencies are proportional to the second derivatives of the potential with respect to elongation of the internal molecular or the external molecule-to-surface bonds. It is interesting to compare their changes to the static lateral

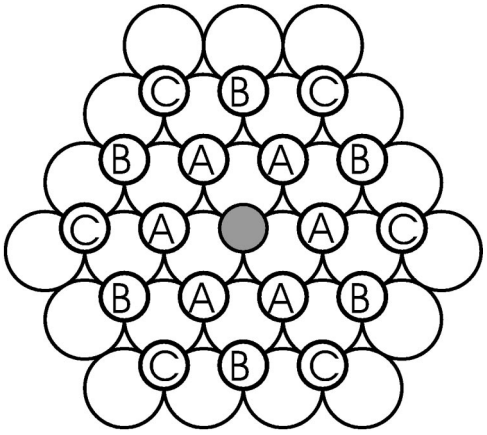

FIG. 12. Arrangement of nearest-neighbor adsorbate sites (A) and next-nearest-neighbor sites (B and C) with distances from the central NO site (gray circle) of 1, $\sqrt{3}$, and 2 substrate units, respectively.

interactions which are responsible for the double-peak structure of the TPD spectrum for the (2×2)-(NO+3O) layer.[28] Based on a lattice gas model we have found nearest-neighbor NO-NO repulsion as well as a (smaller) attractive NO trio interaction necessary for a satisfactory description of the TPD data.[28] Correspondingly, the depth of the NO-Ru potential becomes more shallow with increasing NO coverage. Similarly, with increasing oxygen coverage a lower NO desorption temperature compared to the (2×2)-3O structure has been found [Fig. 3(g)] for low NO coverages, which might be related to a more shallow NO-Ru potential. In both cases the reduced depth of the NO-Ru potential has to be related to a blueshift of the singleton NO-Ru stretching mode. Note that this shift is reversed to the behavior one would expect for a simple Morse potential. Such a reversed chemical shift with potential depth was already found for the O-Ru stretching mode.[14]

V. SUMMARY AND CONCLUSIONS

The vibrational and structural features of dense (NO+O) coadsorbate layers have been studied experimentally using HREELS and TPD. A well-ordered (2×2)-(NO+3O) structure was found, which is characterized by external and internal NO stretching modes at 425 and 1580 cm^{-1}, respectively. Based on the vibrational and thermal desorption features the experimental optimization of the formation of ideal defect-free (2×2)-3O and (2×2)-(NO+3O) layers on Ru(001) is found. For an optimal (2×2)-3O precoverage ($\Theta_O=0.75$ ML) the NO molecules adsorb in the remaining hcp threefold sites of the (2×2)-hole structure surrounded by six nearest-neighbor oxygen adatoms. The dispersion measurements of the external and internal NO stretching modes show downward shifts of 16 and 23 cm^{-1}, respectively, along the $\overline{\Gamma K'}$ direction of the surface Brillouin zone. The dispersion of the NO internal mode is well modeled by dynamical dipole-dipole coupling with vibrational and electronic polarizabilities of 0.42 and 2 $Å^3$, respectively. The dispersion of the external mode (the frustrated translation T_z) is also dominated by dynamical dipole-dipole coupling; however, some contributions from additional substrate-mediated coupling cannot be excluded.

From the comparison of six different (NO+O) structures which all contain exclusively NO in hcp sites the chemical shifts of the internal and external NO stretch with respect to surrounding oxygen atoms or NO molecules have been analyzed. For the internal mode an initial chemical shift of 31 cm^{-1} per next-neighbor oxygen atom is found which drops to 20 cm^{-1} per next-neighbor oxygen atom for the fifth and sixth neighbor. Next-neighbor NO molecules induce a smaller chemical shift of about 12 cm^{-1} per molecule. No chemical shift is found for the internal mode upon variation of next-nearest neighbor sites. In contrast, for the external mode chemical shifts of 5 and 3 cm^{-1} per next-nearest neighbor oxygen atom and next-nearest neighbor NO molecule, respectively, have been extracted.

ACKNOWLEDGMENT

This work was supported by the Deutsche Forschungsgemeinschaft through SFB 338.

*Permanent address: Inst. of General and Inorganic Chemistry, Bulgarian Academy of Sciences, Sofia, Bulgaria.

†Author to whom all correspondence should be addressed, Electronic address: widdra@e20.physik.tu-muenchen.de

[1] C.H.F. Peden and D.W. Goodman, J. Phys. Chem. **90**, 1360 (1986).

[2] D.W. Goodman and C.H.F. Peden, J. Phys. Chem. **90**, 4839 (1986).

[3] C.T. Campbell, Adv. Catal. **36**, 1 (1989).

[4] M. Stichler and D. Menzel, Surf. Sci. **419**, 272 (1999).

[5] K.L. Kostov, P. Jakob, and D. Menzel, Surf. Sci. **331-333**, 11 (1995).

[6] P. Jakob, M. Stichler, and D. Menzel, Surf. Sci. Lett. **370**, L185 (1997).

[7] H.J. Kreuzer, S.H. Payne, P. Jakob, and D. Menzel, Surf. Sci. **424**, 36 (1999).

[8] W. Widdra, T. Moritz, K.L. Kostov, P. König, M. Staufer, and U. Birkenheuer, Surf. Sci. Lett. **430**, L558 (1999).

[9] T.E. Madey, H.A. Engelhardt, and D. Menzel, Surf. Sci. **48**, 304 (1975).

[10] M. Lindroos, H. Pfnür, G. Held, and D. Menzel, Surf. Sci. **222**, 451 (1989).

[11] H. Pfnür, G. Held, M. Lindroos, and D. Menzel, Surf. Sci. **220**, 43 (1989).

[12] F.M. Hoffmann, M.D. Weisel, and C.H.F. Peden, Surf. Sci. **253**, 59 (1991).

[13] I.J. Malik and J. Hrbek, J. Phys. Chem. **95**, 10 188 (1991); J. Vac. Sci. Technol. A **10**, 2565 (1992).

[14] C. Stampfl, S. Schwegmann, H. Over, M. Scheffler, and G. Ertl, Phys. Rev. Lett. **77**, 3371 (1997).

[15] T. Moritz, D. Menzel, and W. Widdra, Surf. Sci. **427**, 64 (1999).

[16] K.L. Kostov, M. Gsell, P. Jakob, T. Moritz, W. Widdra, and D. Menzel, Surf. Sci. Lett. **394**, L138 (1997).

[17] P. Jakob, Surf. Sci. **427-428**, 309 (1999).

[18] H. Conrad, R. Scala, W. Stenzel, and R. Unwin, Surf. Sci. **145**, 1 (1984).

[19] K.M. Neyman, N. Rösch, K.L. Kostov, P. Jakob, and D. Menzel, J. Chem. Phys. **100**, 2310 (1994).

[20] P. Feulner, S. Kulkarni, E. Umbach, and D. Menzel, Surf. Sci. **99**, 489 (1980).

[21] M. Stichler and D. Menzel, Surf. Sci. **391**, 47 (1997).

[22] P. Feulner and D. Menzel, J. Vac. Sci. Technol. **17**, 662 (1980).

[23] H.A. Engelhardt, P. Feulner, H. Pfnür, and D. Menzel, J. Phys. E **10**, 1133 (1977).

[24] T.S. Rahman, A.B. Anton, N.R. Avery, and W.H. Weinberg, Phys. Rev. Lett. **51**, 1979 (1983).

[25] W.J. Mitchell, Y. Wang, M. Schick, and W.H. Weinberg, J. Chem. Phys. **102**, 8185 (1995).

[26] Note that the oxygen coverage is slightly higher than 0.5 as seen by the asymmetric line shape of the O-Ru stretch in Fig. 1(a), which affects also the positions of the modes in Fig. 2(a). The exact values for the well-ordered (2×1)-(NO+O) are 437, 486, 1615, and 1838 cm^{-1}.

[27] T. Moritz, W. Widdra, and D. Menzel (unpublished).

[28] K.L. Kostov, D. Menzel, H.J. Kreuzer, and W. Widdra (unpublished).

[29] J. Braun, K.L. Kostov, G. Witte, L. Surnev, J.G. Skofronick, S.A. Safron, and Ch. Woell, Surf. Sci. **372**, 132 (1997).
[30] K.L. Kostov, T. Moritz, W. Widdra, and D. Menzel (unpublished).
[31] G.D. Mahan and A.A. Lucas, J. Chem. Phys. **68**, 1344 (1978).
[32] P. Jakob and B.N.J. Persson, Phys. Rev. Lett. **78**, 3503 (1997).
[33] A.A. Radzig and B.M. Smirnov, *Reference Data on Atoms, Molecules, and Ions* (Springer, Berlin, 1985).
[34] M.J. Stirniman, W. Li, and S.J. Sibener, J. Chem. Phys. **102**, 4699 (1995).